PERTURBING SHEAR LAYERS IN A TURBULENT WAKE

Diogo Barros, Jacques Borée, Andreas Spohn
Institut Pprime, UPR-3346 CNRS - ISAE-ENSMA - Université de Poitiers
Futuroscope Chasseneuil, France.
diogo.barros@ensma.fr

Bernd R. Noack
LIMSI – CNRS, UPR 3251, Campus Universitare d'Orsay
Rue John Von Neumann, Bât 508, F-91405 Orsay CEDEX, France.
Institut für Strömungsmechanik, Technische Universität Braunschweig
Hermann-Blenck-Straße 37, D-38108 Braunschweig, Germany.

ABSTRACT

The impact of shear layer forcing on the recirculating flow past a turbulent bluff body wake is examined. Flow disturbances generated using active and passive devices modify the evolution of the separated flow from the rear edges of a rectangular geometry. A system of pulsed jets with variable frequency allows us to produce unsteady perturbations, whilst passive boundary layer forcing is obtained by spanwise cylinders with variable diameter. Statistics of velocity fields obtained from particle image velocimetry (PIV) are used to quantify the changes in the recirculating flow. Depending on the forcing frequency or perturbation size, the wake balance is modified due to the enhanced mixing along the forced shear flow. The experimental results show that the symmetry properties of the near wake can be controlled by suitable excitation and provide guidelines for the control of wake-related aerodynamic forces exerted on bluff bodies.

INTRODUCTION

Turbulent shear flows are encountered in numerous configurations of practical relevance such as jets, mixing layers and wakes (Fiedler, 1998). A key mechanism in these flow systems is the growth of convective shear instabilities responsible for mixing. When disturbed, shear layers can amplify a broad range of flow scales evolving into large coherent structures (Ho & Huerre, 1984). In particular, separated shear layers play a crucial role on the wake formation past a bluff body. Their streamwise growth provokes large scale engulfing motions responsible to generate a recirculating flow region in the near wake. The balance of forces in the near wake highly depends on the characteristics of the surrounding shear layers and significantly impacts the topology of the recirculating flow, thereby altering the forces exerted on the rear part of the geometry.

In the present study, we examine experimentally the global effects of shear layer forcing on the large scale recirculating flow behind a rectangular bluff body geometry. Our aim is to understand how shear layer forcing alters the near wake topology by employing active or passive devices.

EXPERIMENTAL METHODS

The experiments are conducted in a subsonic wind-tunnel whose test section dimensions are 2.4 m (width) and 2.6 m (height). Main results are obtained with a constant free-stream velocity $U_o = 15\,\mathrm{ms}^{-1}$ and turbulence intensity of about 0.5 %. The bluff body geometry studied here is shown in figure 1(a). It is placed over a flat plate installed inside the working section, as fully described in (Barros, 2015; Barros *et al.*, 2016*a*). The whole model with height $H = 0.297\,\mathrm{m}$, width $W = 0.350\,\mathrm{m}$ and length $L = 0.893\,\mathrm{m}$ is fixed at a geometrical ground clearance $G = 0.05\,\mathrm{m}$ above this false floor. The ground clearance G is about five times greater than the oncoming boundary layer, which measures $\delta_{99\,\%} \sim 0.034H$ with displacement thickness $\delta^\star \sim 0.004H$ and shape factor $\overline{H} = 1.58$.

The Reynolds number based on the height of the model is $Re_H = U_o H/\nu = 3 \times 10^5$, where ν is the kinematic viscosity of the air at ambient temperature. The coordinate system with x the streamwise, y the transverse or cross-stream and z the spanwise directions has an origin O arbitrarily set on the ground at the base of the bluff body. All physical quantities are normalized by U_o, H and by the dynamic pressure $q_o = 0.5\rho {U_o}^2$, where ρ is the air density at ambient temperature and pressure.

As indicated in figure 1(a, right), the base pressure is quantified by pressure taps distributed on the rear surface. Differential off-set pressure sensors (HCLA 02X5DB) operate in a range of $\pm 250\,\mathrm{Pa}$ with the upstream static pressure p_o as reference. Pressure coefficients are computed by $C_p = (p - p_o)/q_o$. We define the spatial and the time-averaged pressure coefficients respectively by $\langle C_p \rangle$ and $\overline{C_p}$ with acquisition duration of 60 seconds.

Particle image velocimetry (PIV) is used to obtain the velocity field in the wake. A large field of view located in the symmetry plane (z = 0) spans the whole near wake containing the recirculating flow domain. Both the streamwise (u) and the transverse (v) velocity components of the flow are measured by two LaVision Imager pro X 4M cameras. A laser sheet is pulsed with time delays of $120\,\mu\mathrm{s}$ and acquisition of image pairs is sampled at 3.5 Hz. Velocity vectors are processed with an interrogation window of 32×32 pixels and overlap of 50%. The resulting spatial

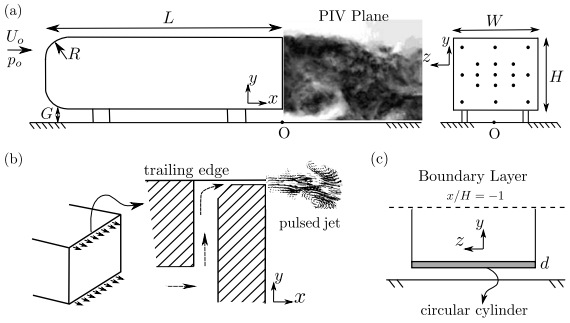

Figure 1. Bluff body geometry and perturbation methods. a) Side and rear views of the bluff body showing the locations of the large PIV field of view and the pressure taps. b) Location of pulsed jet formation for fluidic forcing. c) Rear view of the spanwise cylinder installed at $x/H = -1$.

resolution is approximately 1 % of the model's height. Ensembles of 1000-2500 independent velocity fields are used to compute first and second order statistics. A second PIV set-up allows to perform a zoom close to the upper edge of the model using high-speed PIV (HSPIV). One Photron® SA-Z 1.1 camera with a resolution of 1024×1024 pixels is used to acquire images at a rate of 10 kHz. The laser sheet is generated by a Quantronix MESA 532 nm system. These tests are performed during 8 s and the images are processed with an interrogation window of 16×16 pixels with overlap of 50%.The final spatial resolution is $0.003H$.

SHEAR LAYER FORCING

Wake forcing is generated by employing unsteady jets or passive cylinder perturbations. Pulsed jets with an exit velocity V_j and frequency F_i are produced along the top (F_T) or the bottom (F_B) trailing edges of the geometry, as illustrated in figure 1(b). The entire apparatus designed to obtain these jets, i.e. actuators and pressure supply, is detailed in Barros (2015). The jet amplitude is described by the effective velocity $V_{\text{eff.}} = (\overline{V_j^2})^{0.5}$ which is set to $V_{\text{eff.}} = 7.3\,\text{ms}^{-1}$ in the present measurements. The exit slit with thickness $h = 1 \pm 0.1$ mm is continuous and spans entirely the rear edges, but actuation can be set independently at F_T or F_B. The reader is referred to Barros *et al.* (2016*a*,*b*) for amplitude and lateral actuation effects. For spectral analysis, we scale the actuation frequency by defining the Strouhal number $St_H = F_i H/U_o$.

Spanwise cylinders with variable diameter d can be installed over the lower surface of the model to disturb the underflow boundary layer. Their non dimensional sizes (normalized by H) are $d = 0.027$ and $d = 0.054$. They are installed upstream of the bottom trailing edge ($x/H = -1$) and are illustrated in figure 1(c). We expect that flow separation behind the cylinder and a local change in the boundary layer momentum deficit may affect the growth ratio of the separating shear layer and the entire recirculating flow.

EFFECTS ON THE RECIRCULATING FLOW

The global changes in the near wake are presented when forcing is applied along the top shear layer. As visible in figure 2, the unforced flow presents a large dominating recirculating structure in the clock wise sense. Forcing the upper shear layer using unsteady fluidic actuation enhances this recirculation but strongly depends on the jet frequency (Barros *et al.*, 2016*b*). In figure 2(a), we present contour plots of the cross-stream velocity fluctuations $\overline{v'v'}$ for top slit actuation (F_T) at Strouhal numbers $St_H = \{0.4, 0.8, 1.4, 2.0\}$ and forcing amplitude $V_{j_{\text{eff.}}} \sim 7.3\,\text{ms}^{-1}$.

An overall increase of velocity fluctuations is noticed in all forced shear layers. The main feature is a progressive shift of the zones with high $\overline{v'v'}$ towards the model's edge by the increase of St_H. The velocity variance in the forced shear layers can reach more than twice the values from the unforced flow. It should be mentioned here that $\overline{v'v'}$ also increases along the shear layer near the ground, pointing out a connection between the upper and lower shear flows as well as a global enhancement of turbulent fluctuations in the wake. When the wake is forced at frequencies close to $St_H \sim 0.8$, the amplification of the shear layer along its entire streamwise evolution is observed up to the end of the recirculating region at $x/H \sim 1.5$. This actuation frequency is responsible for decreasing the base pressure coefficient $\langle \overline{C_p} \rangle$ by 12%, while smaller or higher frequencies affects base pressure to a lesser extent, as reported in the table 1.

Table 1. Impact of shear layer forcing (F_T) on the base pressure change and recirculating bubble's length.

St_H	$\Delta\langle \overline{C_p} \rangle$ (%)	L_r
Unforced	-	1.5
0.4	-8.5	1.39
0.8	-12.2	1.34
1.4	-10.7	1.34
2.0	-7.4	1.39

The modifications of the turbulent dynamics along the shear layer strongly impact the large scale entrainment towards the wake. To quantify this, we study the distribution of the time-averaged cross-stream velocity $\overline{v}$ in the near wake. For that, we analyze the mean velocity field when the actuation frequency is $St_H \sim 0.8$, the configuration with the highest increase of drag and cross-stream velocities. More specifically, we identify the regions where $|\overline{v}|$ is maximum, as displayed in figure 2(b).

In figure 2(b,top), three domains corresponding to the higher $\overline{v}$ velocities are illustrated. Region (I) indicates the upward flow adjacent to the rear surface where $\overline{v}$ is greater than 0.06. There is an increase of $\overline{v}$ when actuation is applied, attested quantitatively by the velocity profile at $x/H = 0.05$ (I). At least when considering this data set in the symmetry plane, it strongly suggests that more momentum is deviated towards the wake interior. We confirm this by analyzing the cross-stream velocity field at the end of the recirculating bubble in the regions (II) and (III). They respectively indicate the highest downward ($\overline{v} < -0.2$) and upward ($\overline{v} > 0.06$) velocities in the wake. While the upward motion in region (III) shows modest changes, a significant increase of downward flow is noted in region (II), which is better visible by the velocity profile (II, III) at the streamwise location $x/H = 1.1$. In the forced wake,

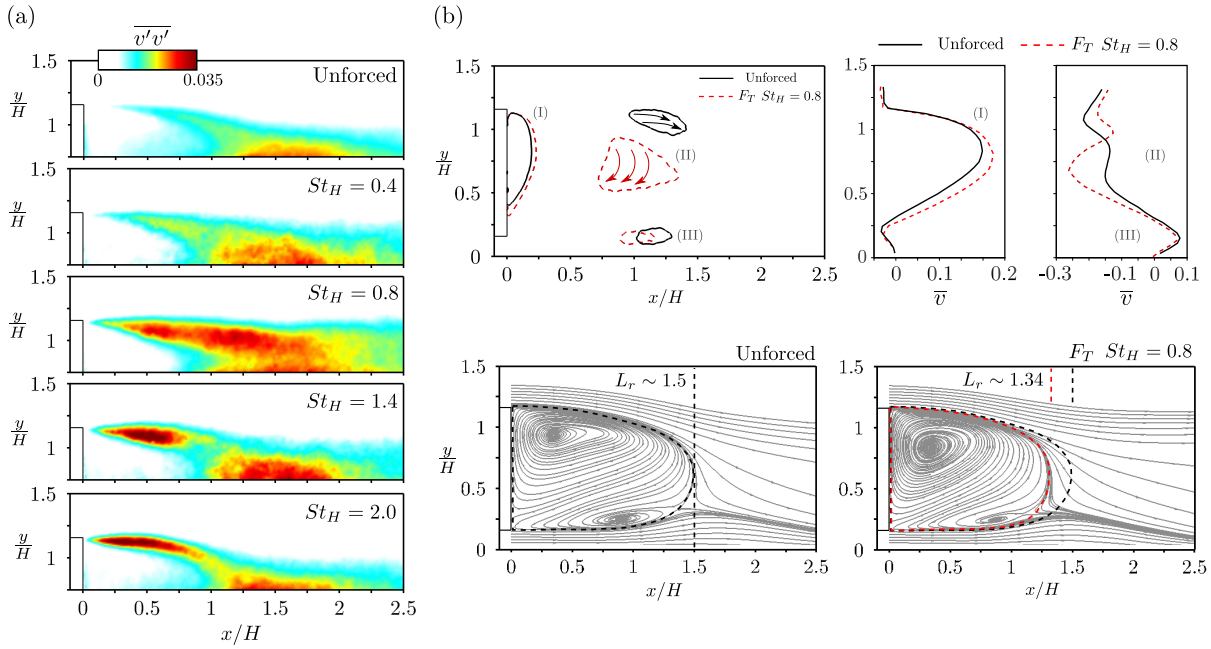

Figure 2. Effects of unsteady forcing (F_T) on the top shear layer. (a) Evolution of $\overline{v'v'}$ as function of forcing frequency St_H. (b) Impact of forcing on recirculating flow inside the wake. Forcing at $St_H = 0.8$ reduces the length of the recirculation zone more than 10%.

both regions are displaced upstream revealing a shortened dead water region as attested by the flow streamlines in figure 2(b,bottom) revealing a decrease of 11% on the bubble's length L_r when actuation is applied. Similarly, the reduction of the bubble's length is the highest for $St_H \sim 0.8$, demonstrating its relationship to the increase of the pressure drag.

SHEAR LAYER FORCING AND TIME SCALES

The pulsed jets are responsible for the modulation of the vorticity flux injected in the shear layers. It is important to understand the spatial structure and length scale of the phase-averaged separated flow to clarify the observed mixing enhancement along the forced shear layer. In figure 3, contour maps of the phase-averaged vorticity ω_z are displayed for selected phases of the actuation cycle when $St_H = 0.8$ with actuation period of $T_i = 0.025$s.

A first phase-locked snapshot illustrates the vorticity sheet of the separated boundary layer prior to the jet emission $t/T_i = 0$. The very beginning of the pulsed jet formation induces a disruption of this vorticity layer ($t = 0.04T_i$). It induces the roll-up of a clockwise rotating structure (I) which is convected downstream as indicated in $t = 0.08T_i$. Inserted pictures at $t = \{0.04, 0.08, 0.12\}T_i$ show the wave-like topology of the velocity vectors due to the roll-up of the main vortex head, whose formation is evidenced at $t = 0.175T_i$ (II). This starting vortex is convected at the shear-layer velocity as illustrated at $t = \{0.28, 0.40, 0.50\}T_i$. A trailing clockwise vortex (III) appears due to the sudden deceleration created by closing the solenoid valve mainly remarked at $t = 0.60T_i$. At this stage ($t = \{0.60, 0.74\}T_i$), both the trailing vortex and the main vortex head are convected. It appears that a pairing of these structures might occur later than $t = 0.90T_i$ due to the higher convective velocity of the trailing vortex. This amalgamation should occur downstream of ($x/H \sim 0.35$) and further details of the process can not be observed with the present field of view. However, measurements at higher actuation frequencies ($St_H = 1.4$ and $St_H = 2.0$) reveal amalgamation of theses structures closer to the trailing-edge.

Since unsteady forcing amplifies the velocity fluctuations $\overline{v'v'}$, it is worth to associate this dynamics to the time scales of the shear layer instabilities. It is shown in Barros *et al.* (2016*b*) that St_θ based on the separating boundary-layer momentum thickness does not scale the broadband range of frequencies around $St_H \sim 0.8$. Indeed, the shear layer frequencies very close to the rear edge are significantly higher than the actuation frequency, as demonstrated by the power spectral density S_v of the velocity signal at $x/H = \{0.04\}$ in figure 4(a).

The power spectral density curves shown in figure 4(b) present the expected decrease of the shear layer frequency for multiple streamwise locations $x/H = \{0.02, 0.04, 0.08, 0.185, 0.27\}$. The frequencies are still higher than the actuation frequency corresponding to the maximum amplification of $\overline{v'v'}$. One may speculate if the jet vortical structures excite the shear layer (SL) modes further downstream. To test this hypothesis, we extract the mean streamwise velocity at $x/H \sim 0.4$ and approximate it to a hyperbolic tangent profile with equivalent maximum peak vorticity. Following Ho & Huerre (1984), we estimate the most amplified frequency for turbulent profiles using $St_\theta \sim 0.022 - 0.024$ and obtain $f_{SL} \sim St_H \sim 0.85$, in good agreement with $St_H \sim 0.8$. By considering its local vorticity thickness δ_ω, we obtain $St_{\delta_\omega} \sim 0.09$ corresponding well to 0.098 reported by Morris & Foss (2003).

This estimate represents fairly well the actuation time scale when compared to the local most amplified shear layer frequency at $x/H \sim 0.4$. Our analysis is supported by past investigations from Oster & Wygnanski (1982) who show that excitation of shear layers with frequencies smaller than the initial most amplified time scales impacts the dynamics further downstream. It is important to stress, however, that the actuation magnitude is significant and the coherent vortical structures might dominate the natural shear development under forcing.

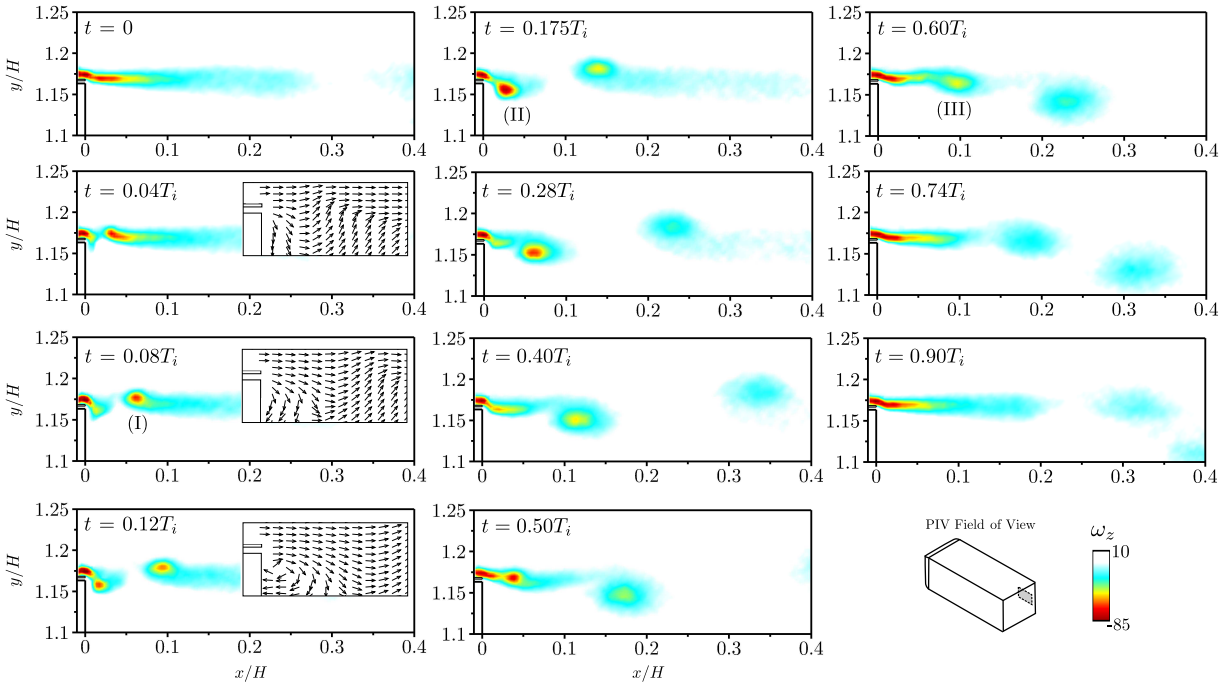

Figure 3. Phase-averaged vorticity field of the forced shear layer with actuation frequency $St_H = 0.8$ (F_T).

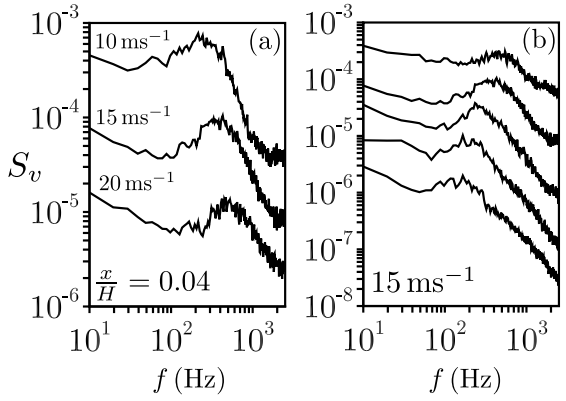

Figure 4. Power spectral density S_v of the transverse velocity. a) S_v at $x/H = \{0.04\}$ for upstream velocities $U_o = \{10, 15, 20\}$ ms^{-1}. b) Downstream evolution of S_v at $x/H = \{0.02, 0.04, 0.08, 0.185, 0.27\}$ for $U_o = 15$ ms^{-1}.

REVERSING THE NEAR WAKE FLOW

While unsteady forcing applied at the upper shear layer enhances the clock wise recirculation of the unforced case, one may envisage to perturb the bottom shear flow to achieve a reverse of the near wake topology. In figure 5(left), we present the effects of F_B forcing with $St_H = 0.2$ and $St_H = 0.8$ on the time-averaged cross-stream velocity field $\overline{v}$. For the smallest actuation frequency, the resulting near wake recirculation appears to be highly symmetric and two counter rotating structures coexist behind the model. On the other hand, actuation at $St_H = 0.8$ promotes a strong wake reversal in which the counter clock wise motion dominates the flow. These results are in agreement with the fact that unsteady forcing close to $St_H = 0.8$ promotes higher mixing in the flow than other frequencies leading to a more important reversal of the recirculation.

To generalize the effects of disturbances, we install passive cylinder devices under the geometry in an attempt to recover the qualitative features of unsteady shear layer forcing. The velocity fields shown in figure 5(right) display a very similar behavior when the size d of the spanwise cylinder is increased. Indeed, imposing stronger perturbations on the boundary layer induce a more significant change on the recirculation geometry.

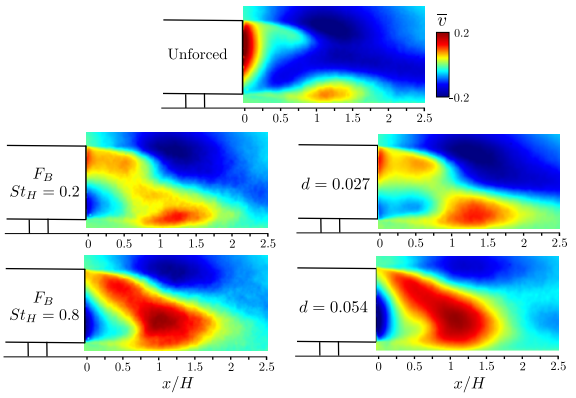

Figure 5. Effects of unsteady (F_B) and passive (d) forcing applied on the bottom shear layer.

The symmetry changes of the recirculating flow in this plane are accompanied by strong modifications of the spanwise flow symmetry. This is demonstrated by the time evolution of the spanwise base pressure gradient $(\Delta C_p)_z$ presented in figure 6 during an acquisition time of ten minutes. While strong asymmetry occurs for the unforced flow and $d = 0.054$ in the symmetry plane ($z = 0$) as evidenced in figure 5(right), spanwise symmetry is measured based

on the pressure gradients. Interestingly, when symmetry is reached by disturbing the flow with $d = 0.027$, strong asymmetric states are originated along the spanwise direction. These asymmetries appear in the form of the bimodal wake reversals which were recently reported by Grandemange *et al.* (2013) and are responsible for a complex competition mechanism inside the recirculating flow region (Barros *et al.*, 2017).

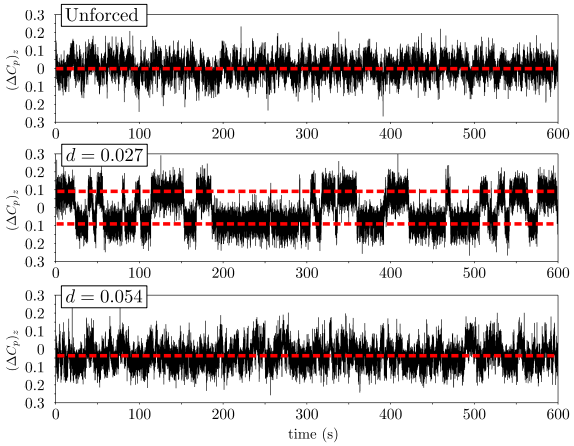

Figure 6. Impact of passive devices on the time evolution of the spanwise wake asymmetries given by $(\Delta C_p)_z$.

CONCLUSIONS

The experimental results presented here highlight general qualitative features of excited shear layers surrounding the recirculating flow contained in the near wake of a bluff body. Independently of the perturbation device, disturbances of different amplitudes and time scales may trigger the local growth of shear layers directly affecting the symmetry properties of large scale motions in the recirculating flow region. Future work will involve the instantaneous flow characterization of the wake reversing process during the application of forcing. A question of interest is to identify the minimum actuation energy necessary to alter the preferred recirculation of the flow. These aspects may provide some guidelines for the development of control strategies aiming wake symmetrization with practical applications in lift, drag and side force control (Brackston *et al.*, 2016; Li *et al.*, 2016).

ACKNOWLEDGMENT

The authors acknowledge the support of PSA Peugeot-Citröen in the OpenLab Fluidics (fluidics@poitiers) and warmly thank J.M. Breux and R. Li for fruitful discussions and assistance during the experiments.

REFERENCES

Barros, D. 2015 Wake and drag manipulation of a bluff body using fluidic forcing. PhD thesis, Ecole Nationale Supérieure de Mécanique et d'Aérotechnique (ENSMA).

Barros, D., Borée, J., Cadot, O., Spohn, A. & Noack, B. R. 2017 Forcing symmetry exchanges and flow reversals in turbulent wakes. *Submitted manuscript* .

Barros, D., Borée, J., Noack, B. R. & Spohn, A. 2016*a* Resonances in the forced turbulent wake past a 3D blunt body. *Phys. Fluids (1994-present)* **28** (6), 065104.

Barros, D., Borée, J., Noack, B. R., Spohn, A. & Ruiz, T. 2016*b* Bluff body drag manipulation using pulsed jets and coanda effect. *J. Fluid Mech.* **805**, 422–459.

Brackston, R. D., de la Cruz, J. M. G., Wynn, A., Rigas, G. & Morrison, J. F. 2016 Stochastic modelling and feedback control of bistability in a turbulent bluff body wake. *J. Fluid Mech.* **802**, 726–749.

Fiedler, H. E. 1998 Control of free turbulent shear flows. In *Flow Control*, pp. 335–429. Springer.

Grandemange, M., Gohlke, M. & Cadot, O. 2013 Turbulent wake past a three-dimensional blunt body. part 1. global modes and bi-stability. *J. Fluid Mech.* **722**, 51–84.

Ho, C. M. & Huerre, P. 1984 Perturbed free shear layers. *Ann. Rev. Fluid Mech.* **16** (1), 365–422.

Li, R., Barros, D., Borée, J., Cadot, O., Noack, B. R. & Cordier, L. 2016 Feedback control of bimodal wake dynamics. *Exp. Fluids* **57** (10), 158.

Morris, S. C. & Foss, J. F. 2003 Turbulent boundary layer to single-stream shear layer: the transition region. *J. Fluid Mech.* **494**, 187–221.

Oster, D. & Wygnanski, I. 1982 The forced mixing layer between parallel streams. *J. Fluid Mech.* **123**, 91–130.